The University of Nottingham
UNITED KINGDOM · CHINA · MALAYSIA

Salerno, G. and Bennett, C.J. and Sun, W. and Becker, A.A. (2017) Residual stress analysis and finite element modelling of repair-welded titanium sheets. Welding in the World . ISSN 0043-2288

Access from the University of Nottingham repository:
http://eprints.nottingham.ac.uk/44476/8/s40194-017-0506-1.pdf

Copyright and reuse:

The Nottingham ePrints service makes this work by researchers of the University of Nottingham available open access under the following conditions.

This article is made available under the Creative Commons Attribution licence and may be reused according to the conditions of the licence. For more details see: http://creativecommons.org/licenses/by/2.5/

A note on versions:

The version presented here may differ from the published version or from the version of record. If you wish to cite this item you are advised to consult the publisher's version. Please see the repository url above for details on accessing the published version and note that access may require a subscription.

For more information, please contact eprints@nottingham.ac.uk

Weld World
DOI 10.1007/s40194-017-0506-1

RESEARCH PAPER

Residual stress analysis and finite element modelling of repair-welded titanium sheets

G. Salerno[1,2] · C. J. Bennett[2] · W. Sun[2] · A. A. Becker[2]

Received: 15 November 2016 / Accepted: 24 July 2017
© The Author(s) 2017. This article is an open access publication

Abstract An innovative finite element modelling approach has been tested to investigate the effects of weld repair of thin sheets of titanium alloy, taking into account a pre-existing stress field in the components. In the case study analysed, the residual stress fields due to the original welds are introduced by means of a preliminary sequentially-coupled thermo-mechanical analysis and considered as pre-existing stress in the sheets for the subsequent repair weld simulation. Comparisons are presented between residual stress predictions and experimental measurements available from the literature, with the aim of validating the numerical procedure. As a destructive sectioning technique was used in the reference experimental measurements, an investigation is also presented on the use of the element deactivation strategy when adopted to simulate material removal. Although the numerical tool is an approximate approach to simulate the actual material removal, the strategy appears to predict a physical strain relaxation and stress redistribution in the remaining part of the component. The weld repair modelling strategy and the element deactivation tool adopted to simulate the residual stress measurement technique are shown to predict residual stress trends which are very well correlated with experimental findings from the literature.

Keywords (IIW Thesaurus) Weld repair · Process modelling · Finite element · Strain-relaxation techniques · Residual stress

Recommended for publication by Commission XV - Design, Analysis, and Fabrication of Welded Structures

✉ C. J. Bennett
chris.bennett@nottingham.ac.uk

[1] Rolls-Royce plc, Ansty, Coventry, CV7 9JR, UK

[2] Gas Turbine and Transmissions Research Group, The University of Nottingham, University Park, Nottingham, NG7 2RD, UK

1 Introduction

Weld repair is a specific application of fusion welding processes that has been adopted across industrial fields to correct anomalies that may arise in structural components from the component manufacturing processes. Furthermore, weld repair can be used where anomalies are introduced through the service life of the component, thus helping to extend the operative life of components. As these are extensively adopted in the nuclear, petrochemical and power generation industries, the main volume of research in this area is related to either aged or deteriorated materials in the case of pipe geometries [1–4]. Although the understanding about repair processes is not extensive, the common approach consists of applying standard established procedures. Little effort is spent to control the residual stresses introduced in the repaired components and the effects of this on the future performance of the structure.

Existing modelling capabilities allow some of the heat effects induced by fabrication welding processes to be predicted. The numerical methodology is well established with a significant amount of works available in the literature. Based on finite element (FE) analysis, the numerical approach is a powerful and well-proven tool for predicting the macro-scale effects of both arc and beam welding processes. An excellent review of the methodology is presented by

Published online: 08 August 2017

Lindgren [5]. Dedicated FE software codes, like Sysweld, have been developed with the aim of applying the numerical strategy in different industrial fields and analysing the residual stress distribution to characterize the structural integrity of the welded joint. Also, cost-effective distortion mitigation is another important example of application in the case of joining thin components.

The suitability of the same numerical strategy in the case of a finite length weld repair has not been clearly demonstrated in the literature and there are currently no universally accepted guidelines for performing such analyses. It is clear that the initial state of a component where a weld repair is needed is not virgin in terms of stress. A pre-existing stress condition could have been caused by any preliminary fabrication process and/or the operative life. There are few investigations on the effects of the repair in a component with a non-zero stress and the extent of the interactions. However, it has been shown that residual stresses due to weld repair tend to exhibit important invariant features because of the severe restraint conditions present in typical repair welding situations, regardless of actual component configurations and materials. Dong et al. [6] analysed several case studies and concluded that finite length weld repairs increase the magnitude of transverse residual stress along the repair when compared to those of initial fabrication welds, they also highlighted a sharp transition from tensile into compressive stress beyond the ends of the repair. The longitudinal stress appears relatively uniform along the repair weld direction, with highly tensile peaks near the refilled slot caused by the strong restraint imposed by the surrounding material [7]. FE numerical strategies presented by Salerno et al. [8] appear to predict residual stresses which are qualitatively consistent with the findings of Dong et al. [6, 7].

Strain-relaxation techniques are very common and reliable approaches to measure residual stresses in the case of both fabrication and weld repaired components in order to investigate the effects of the repair procedures and/or to validate numerical predictions from FE analyses. Deep hole drilling (DHD) is an example of a well assessed and most used technique. The procedure has been studied, analysed and optimized for a long time, and a dedicated standard was developed by ASTM [9]. Although it is very common practice to use the same specimen for residual stress measurements in multiple locations of interest, the standard does not contain any recommendation related to the minimum distance between adjacent holes. The Kirsch solution [10] for stresses at through-holes indicates that little interaction effects would be expected for holes six or more diameters apart. The effect was studied by Hampton and Nelson [11] whose calibration studies (using strain gauges on a 5.18 mm thick steel sample) showed a difference of 7% in the maximum computed stress when the centres of two adjacent blind holes were spaced 4.5 hole diameters apart. Further studies established a stress difference of less than 1% when they were placed 5.7 hole diameters apart. Based on these findings, Grant et al. [12] recommended that the minimum distance between holes should be at least six hole diameters, they also suggested locating strain gauges away from (rather than between) adjacent holes.

In an attempt to simulate the stress release due to the DHD in the material around the hole, a simplified numerical approach was presented by Gârleanu et al. [13]. They did not model the actual material removal, instead they used the "Birth and Death" element tool (element activation/deactivation) [14] to evaluate the strain relaxation due to the hole drilling. A similar approach was also adopted by Jiang et al. [15] . In their study, the strategy, defined as the softening block approach, was used to simulate stage-wise sequential excavations in jointed rock masses (particles or blocks of hard brittle material separated by discontinuity of surfaces, which may or may not be coated with weaker materials). Their results in terms of displacement and stress distribution proved that the approach can be used to simulate the excavation process in such a context. Dong et al. [6] used a layer deactivation scheme to simulate the effect of the local excavation of a repair groove, predicting a redistribution of the original weld residual stresses in the component they analysed.

In this work, the numerical modelling procedure presented by Salerno et al. [8] is tested for validation purposes by simulating a case study of weld repair in titanium alloy thin sheets from the literature. The experimental work conducted by Wu [16] is used as a reference for a qualitative comparison between the predicted and experimental residual stress measurements. The repair procedure is applied on a weld showing an anomaly and the pre-existing residual stresses are considered as the initial condition for the repair model. Three different lengths in the longitudinal direction were considered as the repair cases. As the measurements were conducted with a strain relaxation technique, the element deactivation strategy, as adopted by Dong et al. [6], Gârleanu et al. [13] and Jiang et al. [15], was used to simulate the strain relaxation due to the material removal. The work also includes an investigation of the numerical tool, in order to test its capability to recompute the stress relaxation due to the material removal in a component and, therefore, the new equilibrium condition. Comparison between the numerical and experimental results are presented in terms of longitudinal residual stress for the original weld and the weld repair cases. The weld repair numerical strategy, combined with the element deactivation tool adopted to simulate the destructive technique of the reference residual stress measurements [16], appears to predict trends consistent with the experimental measurements.

2 Methodology

The weld repair process consists of removing a volume of material where an anomaly is found after inspecting a component. A slot is created using a machining operation which is subsequently refilled with a fusion welding process with material deposition. If the anomaly being corrected is small, only a small volume of material is removed, and the remaining part of the structure retains a residual stress state determined by the history of the component. In the present work, a procedure was adopted to simulate the repair of a weld. As the anomaly is relatively small compared to the weld length, it is assumed this has a negligible effect on the residual stress distribution caused by the original joining process. In this section, the case study and the methodology adopted are described. The case study and the residual stress measurements presented in this section and used to test the numerical procedure are part of the work by Wu [16].

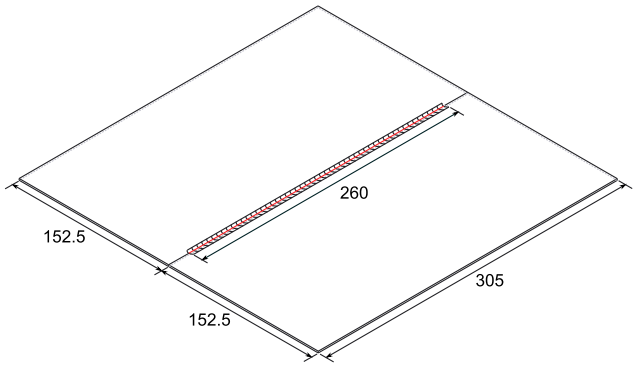

(a) Initial weld.

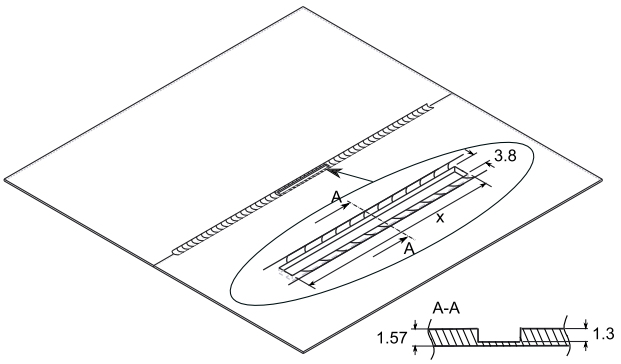

(b) Grinding (A-A cross section of the plate). x is 25, 51 or 102 mm.

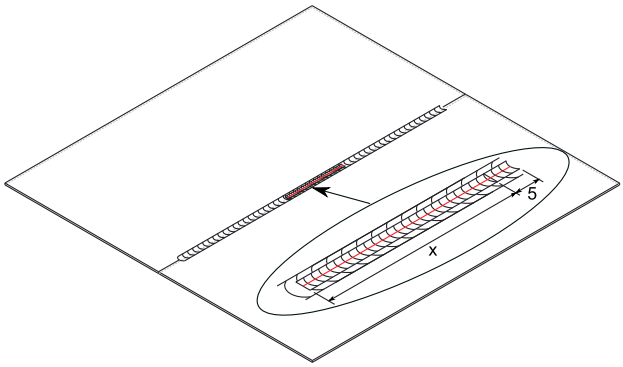

(c) Slot re-filling. x is 25, 51 or 102 mm

Fig. 1 Sequence of the simulated process. Weld paths in *red*. All measurements in millimetre

2.1 Case study

A tungsten-inert gas welding (TIG) was used to join two titanium alloy thin sheets. The sheets were 1.57 mm thick, 305 mm long and 152.5 mm wide. The original weld was 260 mm long, with the start/end located at 22.5 mm from the sheet edges as shown in Fig. 1a. The process parameters are shown in Table 1.

As the welding power was 1140 W, the resulting heat input was 270 J/mm. The material was Ti811 (nominal chemical composition in Table 2).

The anomaly of the weld was ground, creating a groove 1.3 mm deep across the thickness. The groove was centred on the original weld, located as shown in Fig. 1b. Three groove lengths were considered: 25, 51 and 102 mm. The slot was refilled with a single TIG weld pass, with filler deposition. The weld centre line for each TIG weld repair was coincident with the one of the original weld. The repair process was assumed to be equivalent to the initial weld, but the welding power was set to 450 W, resulting in approximately the same heat input as the initial weld. The path for the second weld started 5 mm ahead of the slot as shown in Fig. 1c. The plate was clamped using a rectangular frame with bolts as shown by Wu [16] during both the weld and repair processes.

2.2 Residual stress measurements

The residual stress measurements were conducted by Wu [16] using a destructive sectioning technique, extensively described by Masubuchi [17] and briefly outlined in this section. It is based on the stress-relaxation principle, like semi-destructive hole drilling. The approach involved attaching strain gauges at locations of interest while the specimens were still in the welding frame, using an epoxy

Table 1 Summary of welding parameters

	Weld pass	Repair passes
Velocity (mm s^{-1})	4.23	1.6
Weld power (W)	1140	450

Table 2 Nominal chemical composition of Ti811 (in wt%)

Element	Al	C	H	Fe	Mo	N	O	Ti	V
wt%	7.35–8.35	≤ 0.080	≤ 0.015	≤ 0.03	0.75–1.25	≤ 0.050	≤ 0.12	Balance	0.75–1.25

cement. The electrical resistance of the gauge was initially measured and the corresponding value set as a zero strain. The metal under the gauge was relaxed by removing that volume of plate from the specimen, drilling the material around the edges of the gauge. The net change of electrical resistance measured by the gauge (before and after material removal) was used to determine the elastic strain in the material. This was then converted into residual stress, assuming elastic behaviour and, therefore, using the bulk elastic constants of the alloy (Young's modulus and Poisson's ratio). Multiple measurements were taken from the same specimens, using multiple gauges attached in the locations of interest, obtaining the results shown in Fig. 2.

2.3 Computational model

The numerical model was implemented in the commercial FE code Sysweld as presented by Salerno et al. [8], made up of three macro-steps as shown in Fig. 3. The original weld was simulated using a conventional sequentially-coupled thermo-mechanical analysis. This consists of an initial thermal analysis to predict the thermal field imposed by the welding process into the sheets. The predicted thermal field is then used as an input in the mechanical analysis, leading to the initial stress condition due to the fabrication weld.

The strategy to simulate the weld repair presented by Salerno et al. [8] is briefly summarized in this section. The grinding process to create the excavation was simulated by deactivating elements in the groove (elements death/rebirth [14]), using the coded "status function". The effect is achieved by multiplying the material properties of deactivated elements by a severe reduction factor. The step is purely mechanical and involves the computation of a new equilibrium condition to accommodate the stiffness reduction of the structure. After the deactivation phase, a second sequentially coupled thermo-mechanical analysis was carried out to simulate the repair with filler deposition. Material properties for elements in the slot were defined so that, when reactivated, they continued to have a very low stiffness (1% of the parent material) and their status is identified as the air-phase. A metallurgical model coded in the software was coupled with the thermal one to simulate an artificial material phase change. When the heat source passes, the model converts the air-phase into parent-phase material, which is defined with the mechanical properties of the parent material; key features of the strategy are summarized in Table 3.

In the cases of the initial weld and the shortest and middle length repairs, the deactivation tool was adopted to simulate the material removal where the strain gauges were located

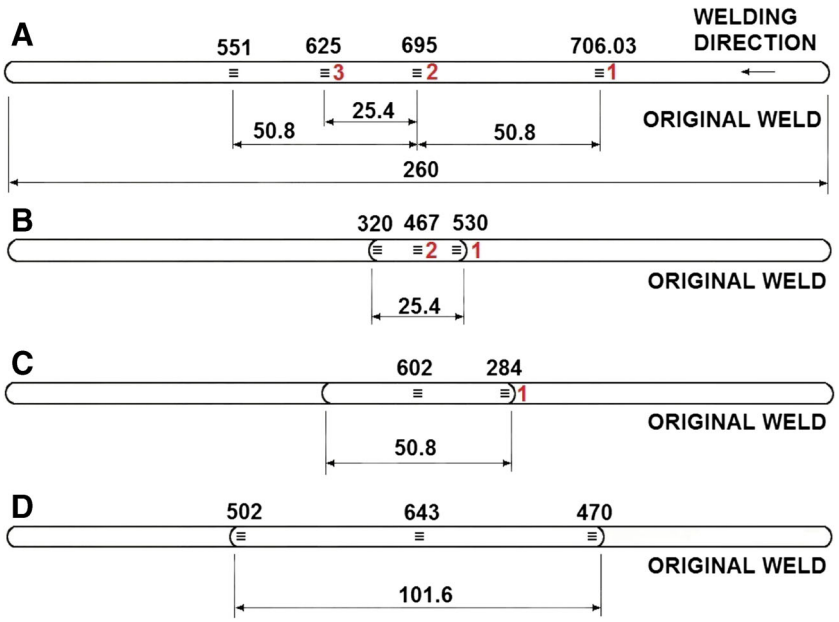

Fig. 2 Longitudinal residual stress measurements (MPa) [16]. **a** Original weld with no repair. **b** Shortest repair. **c** Middle length repair. **d** Longest repair. Length measurements in millimetre. Gauge numbering in *red*

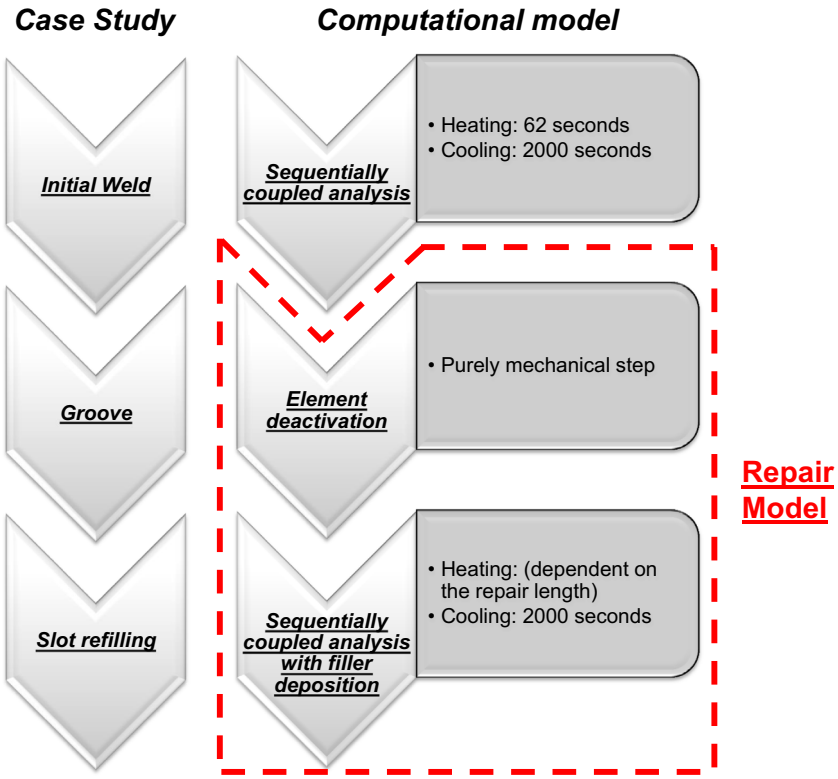

Fig. 3 Outline of the modelling strategy [8]

for the residual stress measurements [16]. As the drilling of the gauge area has a visible effect on the experimental measurements performed in the same specimen, the drilling for the last measurement was not modelled in any of the cases, as the FE predictions could not be compared with experimental results. The material removal was not simulated for the long repair weld as the gauges were sufficiently spaced to ensure the interactions in the measurements were avoided. To investigate the element deactivation tool to simulate material removal, rectangular slots of different areas were removed in the case of the fabrication weld specimen. Referring to the gauge numbering in Fig. 2 and fixing the area of the slot at 30 mm^2, two different removal sequences were analysed. The four cases studied are summarized in Table 4.

In the case of the shortest repair, the area of the slot was fixed at 30 mm^2, simulating the real removal sequence 1-2 as conducted by Wu [16]. In the case of the middle length repair, the area was again fixed at 30 mm^2 and gauge 1 was removed.

To solve both thermal and mechanical non-linear problems, a numerical integration scheme was adopted. A time step, equivalent to one element length travel distance, was chosen for the heating phases of the thermal analyses. This was then set to automatic for the cooling phases. The mechanical steps were run with automatic time incrementation with a maximum time increment of one element length travel distance. In the element deactivation steps, this was reduced to 0.1 s, to ensure convergence of the solution. Non-linear geometric effects were included in all the mechanical analyses, as displacements are large due to the sheets being thin.

2.4 Mesh design

A view of the full mesh is shown in Fig. 4. In the proximity of the weld centre line, the element size was 1.7 × 1.7 × 0.4 mm in order to accurately simulate the heating

Table 3 Overview of the weld repair FE model developed in Sysweld

Physical step	Numerical model
Machining	Status function [18] → *-1*
Slot refilling	Status function → *1*
	Combined with artificial kinetic law

Table 4 Cases studied for the deactivation tool

Case 1	Slot area 6 mm^2	removal sequence: 1-2-3
Case 2 as conducted by Wu [16]	Slot area 30 mm^2	removal sequence: 1-2-3
Case 3	Slot area 72 mm^2	removal sequence: 1-2-3
Case 4	Slot area 30 mm^2	removal sequence: 3-2-1

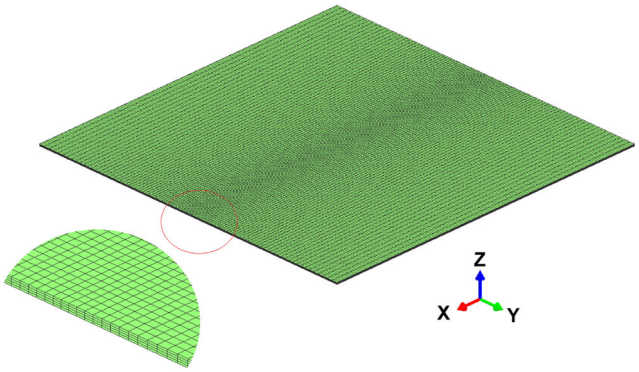

Fig. 4 FE mesh. Zoom on the weld centre line region

process and the steepest temperature gradients close to the torch pass. A mesh transition rule was adopted to increase the element size, moving from the weld centre line to the sheet edges. In the far field, the dimensions were 5 × 1.7 × 0.4 mm. The entire mesh contained 70800 elements and 89890 nodes and was used to solve both the thermal and mechanical problems. Eight-node linear heat transfer brick and eight-node linear brick elements were selected for the thermal and mechanical analyses, respectively.

2.5 Material model

The material investigated by Wu [16] was titanium Ti-8Al-1Mo-1V, an alloy introduced for the first time in 1954. A complete set of temperature-dependent thermal and mechanical properties for this alloy was not available from the literature. As this was necessary to perform the weld simulation in the FE analyses, material properties for the titanium Ti-6Al-4V alloy (nominal chemical composition in Table 5), available from the ESI-Group database, were used. The choice was based on the high similarity of the chemical composition of the two alloys, the small difference for the low temperature properties (as visible in Table 6) and the equivalent liquidus temperature (1500 °C).

Based on the work from Kelly [19], adopted by Deshpande et al. [20], they were set as temperature dependent as shown in Table 7. The FE software adopts a linear interpolation rule for missing values. The melting value was set to 1500 °C, corresponding to the cut-off temperature of the predicted thermal field when transferred into the mechanical model. The effect of latent heat during melting and solidification was not accounted for.

The total strain is decomposed as follows:

$$\varepsilon = \varepsilon^e + \varepsilon^p + \varepsilon^{th} \tag{1}$$

where the three components on the right hand side of Eq. 1 are the elastic, plastic and thermal strains, respectively. The elastic strain was modelled with the isotropic Hooke's law, while yielding was defined using the von Mises criterion. A rate-independent model with a linear isotropic hardening behaviour was assumed for the plastic material properties. The thermal strain is computed by means of the temperature-dependent mean expansion coefficient. The weld pool was simulated in the mechanical analysis by zeroing the total strain when the temperature exceeded the selected melting value. As it was not possible to adopt the actual material properties of the alloy analysed in the reference work [16], experimental measurements were only used to analyse the trends of the longitudinal residual stress predicted from the FE code.

2.6 Thermal and mechanical boundary conditions

The environment and initial temperature of the sheets were both set to 20 °C. Convection and radiation effects were both included as heat loss mechanisms using the Newton and Stefan-Boltzmann laws, respectively. The second effect dominates at higher temperatures near and in the weld zone, while the first effect is more relevant for lower temperatures, outside the fusion zone. The convective and emissivity coefficients were set to 25 W/m^2 and 0.8, respectively [20].

The double ellipsoid heat source model developed by Goldak et al. [21] was selected to simulate the heating for the initial TIG process. The heat power is distributed as following:

$$Q_f(x, y, z, t) = f_f \cdot Q_0 \cdot e^{-z^2/a^2} e^{-y^2/b^2} e^{-(x-vt)^2/c_f^2} \tag{2}$$

$$Q_r(x, y, z, t) = f_r \cdot Q_0 \cdot e^{-z^2/a^2} e^{-y^2/b^2} e^{-(x-vt)^2/c_r^2} \tag{3}$$

where the subscripts f and r denote the front and rear regions of the ellipsoid respectively, f defines the fraction of the heat power deposited in either region (with $f_1 + f_2 = 2$). a, b, c_f and c_r are geometrical parameters of the heat source as shown in Fig. 5 and set as in Table 8, Q_0, v, t are the effective power input, welding velocity, and time, respectively.

Table 5 Nominal chemical composition of Ti64 (in wt%)

Element	Al	C	H	Fe	N	O	Ti	V
wt%	5.5–6.5	≤ 0.080	≤ 0.0125	≤ 0.025	≤ 0.030	≤ 0.13	Balance	3.5–4.5

Table 6 Ti-811 and Ti-64 material properties at 20 °C

	Conductivity (J/m °C s)	Specific heat (J/Kg °C)	Density (Kg/m^3)	Yield stress (MPa)	Thermal expansion coefficient (10^{-6} °C^{-1})	Young's modulus (GPa)
Ti-811	0.006	502	4370	930	8.5	120
Ti-64	0.007	540	4420	900	8.5	113.8

After the plate cooled down to 20 °C, the heating process for the repair pass was simulated using a 2D Gaussian distribution of the heat power, chosen for the reduced number of parameters to be selected. In this case, the power Q was distributed as:

$$Q = Q_0 \cdot e^{-(y)^2/r_0^2} e^{-(x-vt)^2/r_0^2} \tag{4}$$

where r_0 is the Gaussian radius, set to 6 mm to ensure the fusion zone enclosed the excavated groove. The effective power input must be computed by multiplying the welding power (Table 1) by the arc efficiency η. This can assume a value in a wide range for a TIG process (0.36 to 0.90), as it depends on several factors, such as material, arc length, torch velocity and so on. A value of 0.75 was selected both for the initial and repair weld, based on the material analysed [22].

Secondary effects due to the clamping system were not modelled. A simplified constraint was applied in the mechanical analyses to simulate the effect of the frame. This was achieved by assuming a rigid clamp along the Z direction in the region of the frame, as shown in Fig. 6. An artificial boundary condition was also necessary to prevent rigid body motion. This was applied on the nodes highlighted in black as following:

- Node A constrained in the X,Y,Z direction
- Node B constrained in the Y,Z direction
- Node C constrained in the Z direction

3 Results

3.1 Thermal analyses

The predicted thermal histories due to the original weld are presented in Fig. 7.

These are extracted at 7, 8.5 and 10 mm from the weld centre line on the top surface of the sheet, at the mid-length of the weld. The positive and negative gradients in trends of temperature are a clear effect of the heat source pass and cooling down. The gradients in the trends due to the torch approaching become steeper moving towards the weld pass and also, the maximum temperature increases. The highest peak clearly occurs, as expected, at the shortest distance from the weld centre line. In Fig. 8, the predicted thermal

Table 7 Material properties of titanium Ti64 [19]

Temperature (°C)	Conductivity (J/m °C s)	Specific heat (J/Kg °C)	Density (Kg/m^3)	Yield stress (MPa)	Thermal expansion coefficient (10^{-5} °C^{-1})	Young's modulus (GPa)	Poisson's ratio
20	7	540	4420	900	0.85	113.8	0.342
100	–	–	–	800	–	–	0.342
200	–	–	–	700	–	108	0.342
300	–	–	–	635	–	–	0.342
400	–	–	–	550	–	100	0.342
500	–	–	–	470	–	–	0.342
600	–	–	–	–	–	94	0.342
1000	–	–	–	138	–	80	0.342
1200	–	–	–	34	–	–	0.342
1400	–	–	–	–	–	–	0.342
1500	–	–	–	5	1568	5	0.342
1650	–	–	4190	–	–	1	0.342
1800	3	940	–	–	–	–	0.342

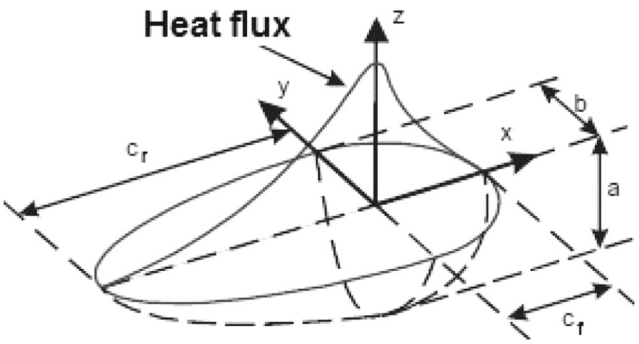

Fig. 5 Schematic model for double ellipsoid heat source [21]

histories are shown in the case of the repair weld passes at the same distances from the weld path and the same locations as before.

As expected, the maximum temperatures at each location are lower than the corresponding ones for the initial weld, as the weld power was less. Due to the lengths of the repair passes being different, the thermal histories appear shifted in time. Also, in the case of the shortest pass, the maximum temperature is slightly lower than the longer passes. A comparison between the fusion zones predicted for the initial weld and repair passes is shown in Fig. 9, as seen from the top view. As an effect of the different torch velocities, the weld pool and the isothermal curves appear to have an ovoid shape in the case of the initial weld, tending to a circle/ellipse in the case of the repair passes. The effect of the torch velocity is also visible on the positive gradients of the thermal histories as well (Figs. 7 and 8), when the heat source approaches the location of interest. These tend to be steeper in the case of the initial weld than the repair passes because of the higher weld velocity.

3.2 Mechanical analyses

As the strain gauges have finite dimensions, the experimental measurements conducted by Wu [16] can be considered as an average of the stresses where the gauges were located [17]. The longitudinal stresses predicted from the FE model were considered along all the longitudinal paths whose nodes fell in the area where the gauges were located (Fig. 10). Data were then averaged at each x location in order to show a consistent comparison between predictions and experimental results. The approach was adopted for all the numerical mechanical results presented in this section.

Table 8 Geometrical parameters of the double ellipsoid

	a	b	c_f	c_r	f_f	f_r
Original weld	1.57	3.0	1.3	2.7	1.2	0.8

Figure 11 shows the longitudinal residual stress due to the initial welding process. The drilling refers to the removal of the material around the gauges. The predicted longitudinal stress does not appear to have a decreasing trend as is visible in the experimental results. However, when the material removal was included in the FE model by means of the element deactivation tool, the FE code lowered the stress to zero in the location where gauges were located (Fig. 10). The area close to the gauge locations is clearly affected as well, showing a decrease in the stress dependent on the distance where the material was drilled. The overall effect on the stress is the apparent decrease in the trend, as visible in the experimental measurements.

When the extent of the area removed changes, the effect on the stress in the neighbouring material changes as well. This is visible in Fig. 12 where, the effect of increasing and decreasing the extent of the deactivated area on the longitudinal stress is shown. It is clear that the deactivation tool predicts a more noticeable stress relieving effect in case 3 (largest gauge area). Also, the material shows the relieving effect at a longer distance from the removed area when this is larger. The removal sequence plays an important role in the stress redistribution as well. If one compares Fig. 11 (case 2) and 13 (case 4), it is quite evident that the distribution of the stress after the removal of the first 2 gauges is different as the removal sequence was inverted. However, it is worth highlighting that the stress distribution is equivalent after the last gauge is removed (blue curves).

In Fig. 14, the longitudinal residual stress due to the shortest weld repair is compared with the experimental results. Again, the experimental measurements show an apparent decreasing trend, which is visible in the FE predictions when the simulation of the gauge removal is included in the analysis.

Figures 15 and 16 show the longitudinal stress for the longer repairs. In the case of the middle length repair, the FE model showed that a spacing of 25.4 mm was sufficient to avoid interactions in the measurements. Therefore, the effects of the material removal were not simulated in the case of the longest repair. Good agreement is visible for the middle length repair, with the predicted trend appearing to be consistent with the measurements both at weld centre and close to the end of the groove. In the case of the longest length repair, the numerical predictions again show a trend in good agreement with the experimental measurements at the start and the end of the repair, but less consistency is found at the weld centre where the magnitude of the experimental value appears significantly higher than the FE predictions.

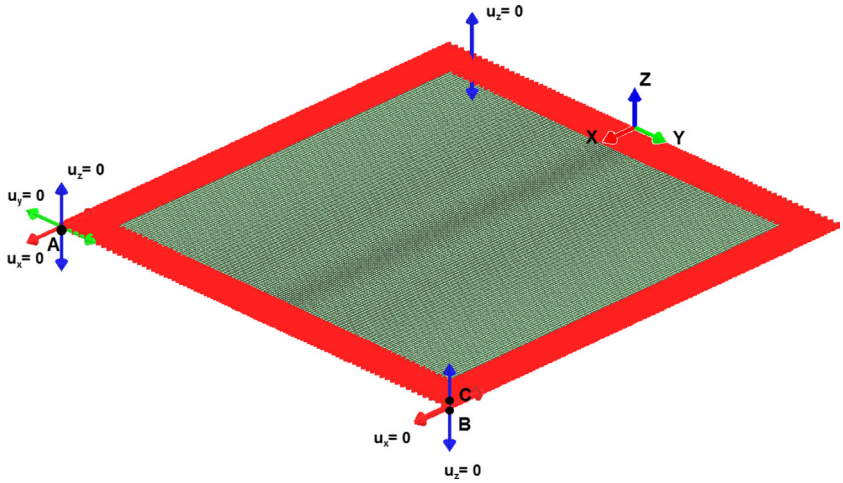

Fig. 6 Mechanical boundary conditions

4 Discussion

The results from the thermal analysis of the initial welding process demonstrate the well-known capability of the double ellipsoid heat source to simulate the heating process due to a TIG weld pass. In the case of thin plates, it is a common choice to adopt a 2D Gaussian power distribution, because it is easy to manipulate with a low number of parameters to be set, giving accurate results and correctly predicting the heating phase due to the welding process. However, in the case of high weld speeds, it fails to capture the ovoid shape of the weld pool as the heat power is distributed in a disk. Also, thermal histories in the weld heat affected zone would not exhibit the sharp temperature increase due to the torch approach, predicting a smoother gradient. The 3D double ellipsoid from Goldak bypasses this incongruity, thanks to the better control of the power distribution. The effect was easily modelled by assigning a higher heat power fraction to the front semi-ellipsoid.

As the weld velocity was lowered for the repair passes, the 2D Gaussian heat source model could be adopted and was chosen here. The welding power was reduced to ensure the thermal effects of the weld repair were confined in the area close to the groove.

If a weld torch were moved on a plate of infinite length, the heating phase could be considered stationary. A good

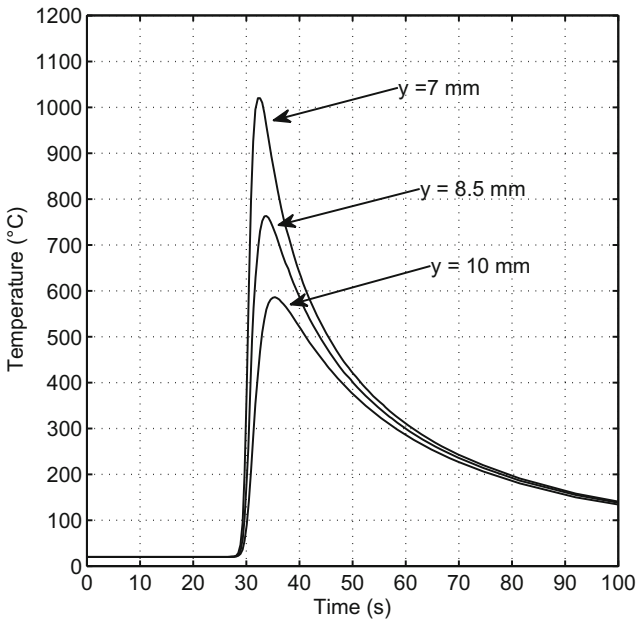

Fig. 7 Initial weld, predicted thermal cycles at 7, 8.5 and 10 mm from the weld centre line at the mid-length of the weld

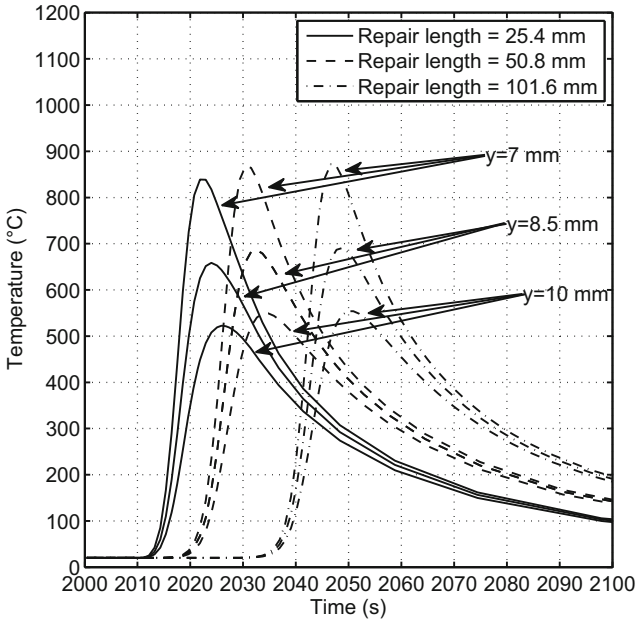

Fig. 8 Repair weld, predicted thermal cycles at 7, 8.5 and 10 mm from the weld centre line at the mid-length of the weld

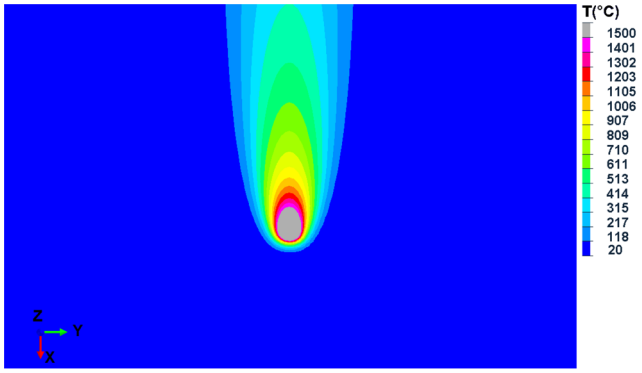

(a) Initial weld.

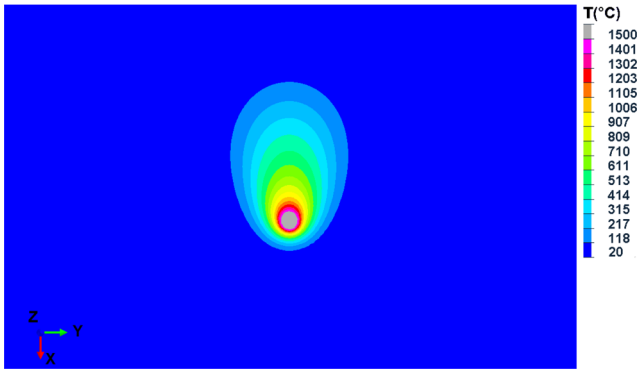

(b) Repair weld.

Fig. 9 Weld pool, top view

approximation of the process is the analytical solution from Rosenthal [23]. This shows that thermal histories at the same distance from the weld centre line would be analogous (in trends and magnitude) but simply shifted in time. In the case of the longer repair passes, the process lasts a sufficient

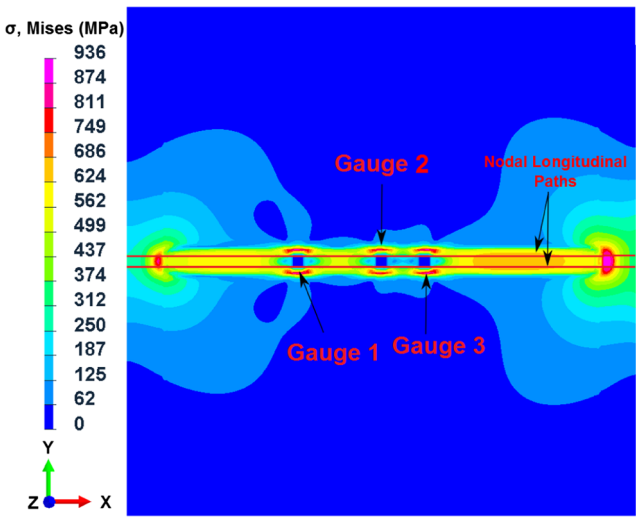

Fig. 10 Location of nodal longitudinal paths which enclose all the paths selected for the stress analysis

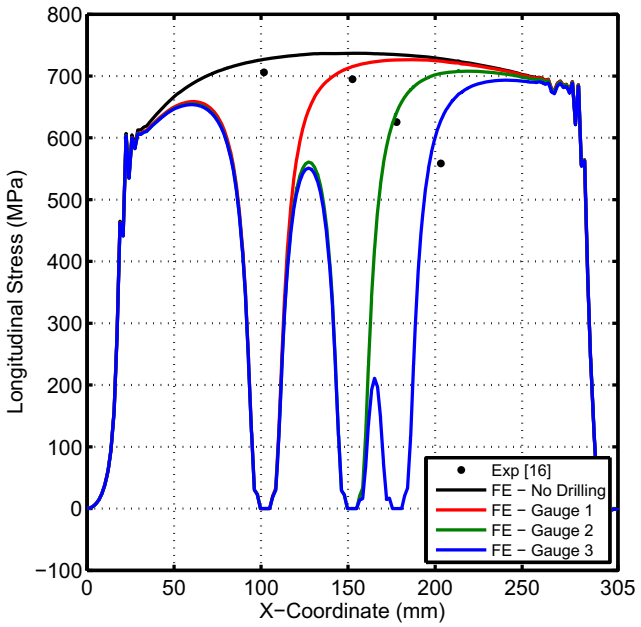

Fig. 11 Longitudinal residual stress due to the initial welding process

time to reach a stationary condition. Therefore, the thermal history appears simply shifted in time as in the case of the analytical solution. In the case of the shortest repair pass, the process is so short, there is not enough time to reach a stationary state. As a consequence, the maximum temperature registered at the same distances from the weld centre line appears slightly lower (approximately twenty degrees) than the longer repair passes.

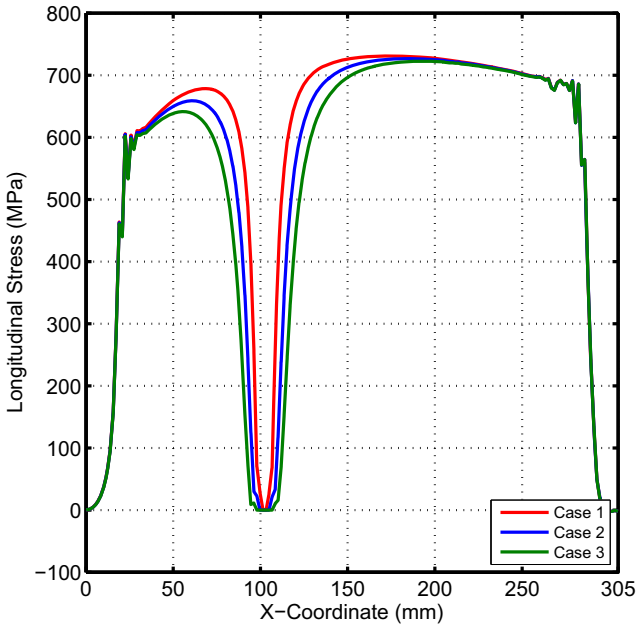

Fig. 12 Effect of the removed area on the longitudinal stress distribution

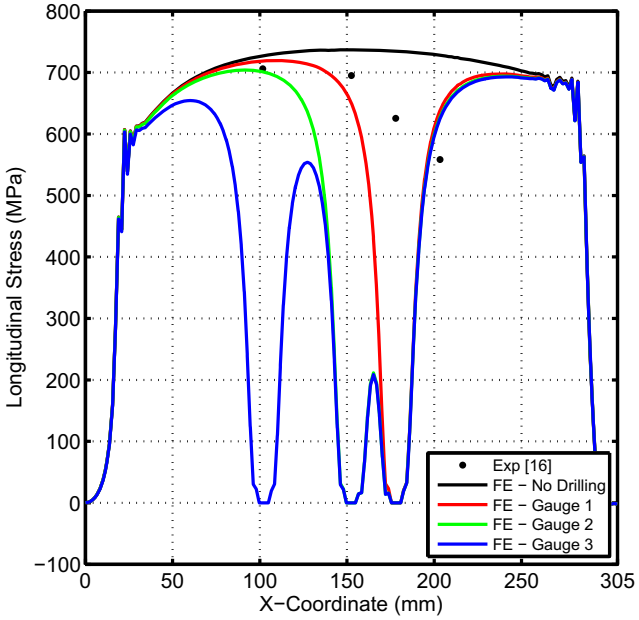

Fig. 13 Effect of the removal sequence on the longitudinal stress distribution

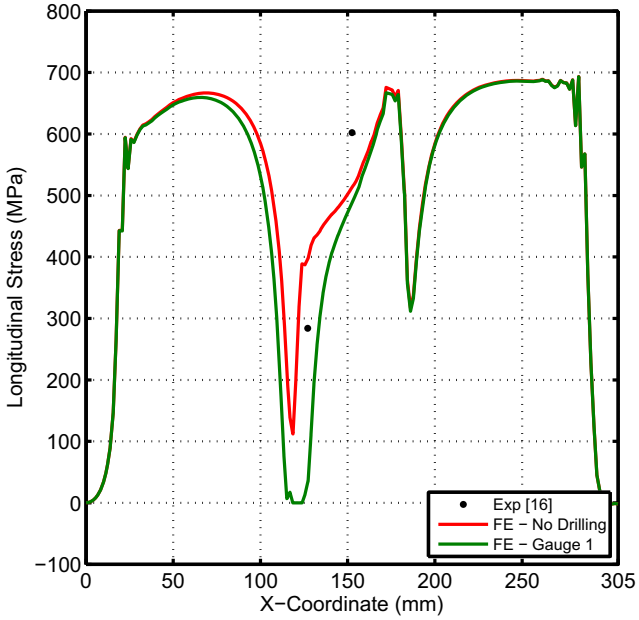

Fig. 15 Longitudinal residual stress, middle length repair. Drilling area set as in case 2

The analysis of the measured longitudinal residual stress along the weld line shows an unjustified decreasing trend, both in the case of the initial weld and the shortest repair pass. Since the welding process was automatic and the constraints of the system were symmetrical, the authors judged the decreasing trend in the measured longitudinal residual stress not coherent. A possible reason to explain the incongruity is given by considering the stress relief caused by the drilling of the plate areas where the strain gauges were located. The sectioning technique adopted for the experimental measurements is based on the same principle (strain relaxation) of the semi-destructive DHD. Although the ASTM standard [9] for the DHD procedure does not give any recommendation in spacing the holes for multiple measurements in the same test specimen, Hampton and Nelson [11] proved that a rule of 6 holes diameters

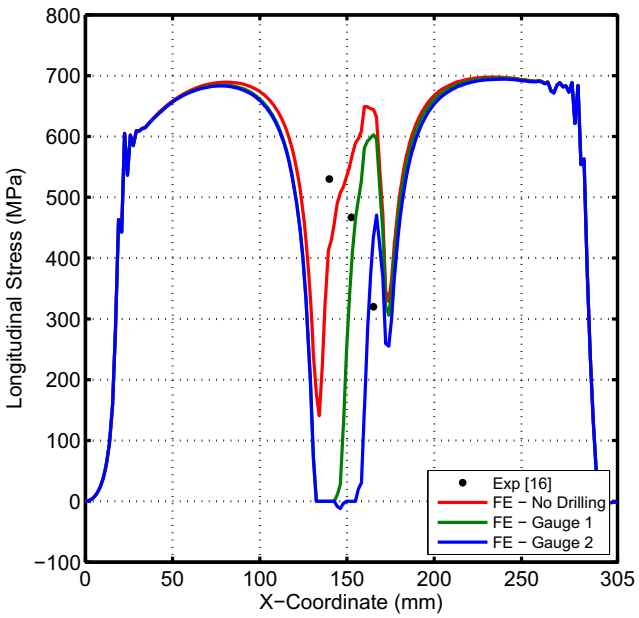

Fig. 14 Longitudinal residual stress, shortest repair. Drilling area set as in case 2

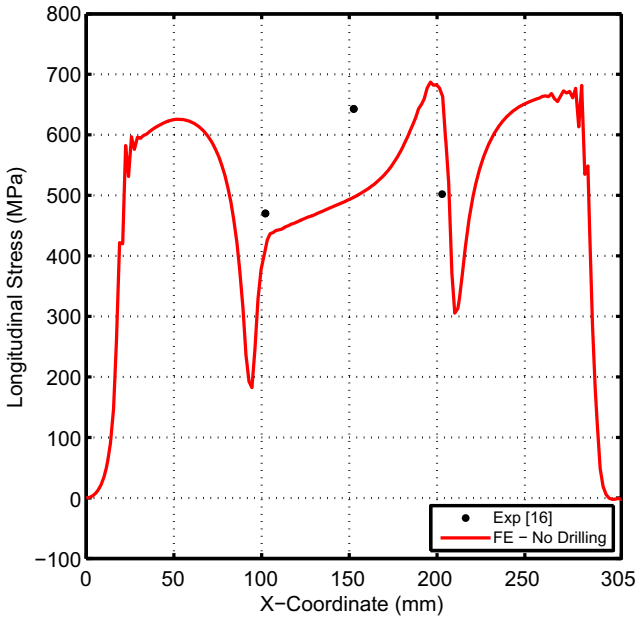

Fig. 16 Longitudinal residual stress, longest repair. Drilling area set as in case 2

should be adopted to avoid interaction between the measurements. This aspect was not considered by Wu [16] when the experimental measurements were taken. As no rule was adopted to space the locations of the holes drilled, and entire portions of material (relatively large) were removed from the specimens, the measured residual stress after the first drilling in the plate must be considered both an effect of the welding processes and the stress relaxation caused by the material removal. The effect is clear in the case of both the initial and the shortest repair, where the spacing was not sufficient to avoid interactions. It is not as evident for the middle and longest repair because of the reduced number of measurements and also the longer distance between the hole locations. The discrepancy between the FE predictions and the measurement of the residual stress for the longest repair (in the middle of the plate) is possibly due to an incapability of the FE model to capture the stationary state of the process. As the repairs were carried out on relatively short distances, the FE model tends to overestimate (or underestimate) the interactions between the start and end point of the repair passes.

Drilling holes in the same test specimen in order to obtain multiple residual stress measurements is a good approach to avoid uncertainties caused by the test repeatability. However, a spacing rule must be adopted between the locations where measurements are taken. When the element deactivation tool was adopted in the numerical model to simulate material removal, this imposed a very low stiffness for the deactivated area and the corresponding stress was therefore zeroed. As a consequence, a visible decrease of the longitudinal stress was caused in the neighbouring region. The FE software code redistributes the stress in the model because a new equilibrium condition has to be computed. Although the approach neglects the actual effects of the drilling process, the stress redistribution due to the simplified numerical strategy appears consistent with the experimental measurements. It can be then be used to define the minimum spacing between holes to avoid misleading measurements. As one should expect, the region affected by the deactivation effect is larger when the extent of the area removed increases, and the stress relaxation is clearly more pronounced. However, as the FE analysis simply computes a new equilibrium condition due to the stiffness reduction in the model, analogous stress distributions have to be expected in the case when the same regions of elements were deactivated (even if different deactivation sequences were adopted).

5 Conclusions

- The numerical modelling strategy presented by Salerno et al. [8] was tested to simulate weld repair of thin sheets, for a different material (titanium alloy) and repair location. The case analysed is part of the study from Wu [16] and experimental data were used as a reference for the numerical predictions. The numerical results are in very good agreement with experimental measurements, demonstrating the feasibility of adopting the model for different materials and/or repair locations.
- Conclusions addressed by Wu in terms of a potential relation between residual stress and repair length cannot be considered valid as the experimental measurements were misrepresented by the destructive technique adopted to determine the residual stresses. However, the FE modelling strategy developed was able to predict longitudinal stress coherent with experimental results.
- It is not possible yet to draw a general conclusion on the effects and interaction of an initial stress state in a component and a weld repair, unless a proper study is conducted to investigate the specific situation. The numerical model tested in the present work can certainly be adopted as a valid investigation tool to quantify the significance of the interaction and to bypass the uncertainty related to neglecting or considering an initial stress state in the component.
- The element deactivation tool was adopted in the FE model to simulate the material removal due to the experimental technique used for the reference residual stress measurements. The numerical tool has been tested to simulate the removal of different extents of material in the same removal sequence and vice-versa. The stress redistribution appears to properly capture the actual stress relieving in proximity of the drilled areas.

Acknowledgements The authors wish to thank Rolls-Royce Plc for their financial support of the research, which was carried out at the University Technology Centre in Gas Turbine Transmission Systems at The University of Nottingham.

Open Access This article is distributed under the terms of the Creative Commons Attribution 4.0 International License (http://creativecommons.org/licenses/by/4.0/), which permits unrestricted use, distribution, and reproduction in any medium, provided you give appropriate credit to the original author(s) and the source, provide a link to the Creative Commons license, and indicate if changes were made.

References

1. Dong P, Zhang J, Bouchard PJ (2002) Effects of repair weld length on residual stress distribution. J Press Vessel Technol 124(1): 74–80
2. Bouchard PJ, George D, Santisteban JR, Bruno G, Dutta M, Edwards L, Kingston E, Smith DJ (2005) Measurement of the residual stresses in a stainless steel pipe girth weld containing long and short repairs. Int J Press Vessel Pip 82(4):299–310

3. Elcoate CD, Dennis RJ, Bouchard PJ, Smith MC (2005) Three dimensional multi-pass repair weld simulations. Int J Press Vessel Pip 82(4):244–257
4. Vega OE, Hallen JM, Villagomez A, Contreras A (2008) Effect of multiple repairs in girth welds of pipelines on the mechanical properties. Mater Charact 59(10):1498–1507
5. Lindgren LE (2006) Numerical modelling of welding. Comput Methods Appl Mech Eng 195(48):6710–6736
6. Dong P, Hong JK, Bouchard PJ (2005) Analysis of residual stresses at weld repairs. Int J Press Vessel Pip 82(4):258–269
7. Dong P, Hong JK, Rogers P (1998) Analysis of residual stresses in al–li repair welds and mitigation techniques. Welding Journal - New York 77:439s–445s
8. Salerno G, Bennett C, Sun W, Becker A (2016) Finite element modelling strategies of weld repair in pre-stressed thin components. J Strain Anal Eng Des 51(8):582–597
9. Standard ASTM E837-08 (2008) Standard test method for determining residual stresses by the hole drilling strain gage method. ASMT international, West Conshohocken, PA
10. Kirsch G (1898) Theory of elasticity and application in strength of materials. Zeitschrift des Vereins Deutscher Ingenieure 42(29):797–807
11. Hampton RW, Nelson DV (1992) On the use of the hole-drilling technique for residual stress measurements in thin plates. J Press Vessel Technol 114(3):292–299
12. Grant PV, Lord JD, Whitehead PS (2006) The measurement of residual stresses by the incremental hole drilling technique. Measurement Good Practice Guide No 53
13. Gârleanu G, Popovici V, Gârleanu D, Arsene D (2010) Modeling by finite element method blind hole drilling method. In: Proceedings of the 3rd WSEAS international conference on finite differences–finite elements–finite volumes–boundary elements. Wisconsin, USA, pp 82–85
14. Teng TL, Chang PH, Tseng WC (2003) Effect of welding sequences on residual stresses. Comput Struct 81(5):273–286
15. Jiang Q, Zhou C, Li D, Yeung MR (2012) A softening block approach to simulate excavation in jointed rocks. Bull Eng Geol Environ 71(4):747–759
16. Wu KC (1981) Residual stress measurements in repair-welded titanium sheets. Welding Research Supplement, pp 12s–18s
17. Masubuchi K (1980) Analysis of welded structures: residual stresses, distortion, and their consequences, vol 33. Pergamon Press
18. SYSWELD (2014) Reference manual. ESI Group, France
19. Kelly SM (2004) Thermal and microstructure modeling of metal deposition processes with application to ti-6al-4v. PhD thesis, Virginia Polytechnic Institute
20. Deshpande AA, Short AB, Sun W, McCartney DG, Xu L, Hyde TH (2012) Finite element-based analysis of experimentally identified parametric envelopes for stable keyhole plasma arc welding of a titanium alloy. J Strain Anal Eng Des 47(5):266–275
21. Goldak JA, Chakravarti A, Bibby M (1984) A new finite element model for welding heat sources. Metall Trans B 15(2):299–305
22. Stenbacka N, Choquet I, Hurtig K (2012) Review of arc efficiency values for gas tungsten arc welding. In: IIW commission IV-XII-SG212, intermediate meeting, BAM, Berlin, Germany, 18-20 April, pp 1–21
23. Rosenthal D (1941) Mathematical theory of heat distribution during welding and cutting. Welding Journal - New York 20(5):220s–234s